5472–5481 *Nucleic Acids Research, 2008, Vol. 36, No. 17* *Published online 21 August 2008*
doi:10.1093/nar/gkn529

Core flexibility of a truncated metazoan mitochondrial tRNA

Ashley A. Frazer-Abel[1] and Paul J. Hagerman[2,*]

[1]National Jewish Health, Denver, CO 80206 and [2]Department of Biochemistry and Molecular Medicine, University of California, Davis, School of Medicine, Davis, CA 95616, USA

Received May 29, 2008; Revised July 29, 2008; Accepted August 1, 2008

ABSTRACT

Secondary and tertiary structures of tRNAs are remarkably preserved from bacteria to humans, the notable exception being the mitochondrial (m) tRNAs of metazoans, which often deviate substantially from the canonical cloverleaf (secondary) or 'L'-shaped (tertiary) structure. Many metazoan mtRNAs lack either the TψC (T) or dihydrouridine (D) loops of the canonical cloverleaf, which are known to confer structural rigidity to the folded structure. Thus, the absence of canonical TψC–D interactions likely results in greater dispersion of anticodon-acceptor interstem angle than for canonical tRNAs. To test this hypothesis, we have assessed the dispersion of the anticodon-acceptor angle for bovine mtRNA^{Ser}(AGY), which lacks the canonical D arm and is thus incapable of forming stabilizing interarm interactions. Using the method of transient electric birefringence (TEB), and by changing the helical torsion angle between a core mtRNA bend and a second bend of known angle/rigidity, we have demonstrated that the core of mtRNA^{Ser}(AGY) has substantially greater flexibility than its well-characterized canonical counterpart, yeast cytoplasmic tRNA^{Phe}. These results suggest that increased flexibility, in addition to a more open interstem angle, would allow both noncanonical and canonical mtRNAs to utilize the same protein synthetic apparatus.

INTRODUCTION

The cloverleaf secondary structure and concomitant 'L' tertiary structure of tRNAs is remarkably conserved from bacteria to humans, but is not universal. The exceptions are found in the mitochondria of metazoans. Some of these tRNAs exhibit minor additions or alterations while others lack an entire arm of the cloverleaf. Measurements in our laboratory have demonstrated that these noncanonical variations in secondary structure lead to substantial variations in tertiary structure (1–3). In particular, the variant mitochondrial tRNAs (mtRNAs) exhibit apparent angles between their anticodon and acceptor stems (~120–140°) that are substantially larger than the ~80–90° exhibited by canonical yeast tRNA^{Phe} (1–5).

What remains unknown is the influence that these structural variations have on the overall flexibility of the mtRNA core. Previous measurements of the flexibility of the canonical yeast tRNA^{Phe} revealed that in the presence of millimolar magnesium concentrations, the tRNA core, as reflected in the anticodon-acceptor interstem angle, remains quite rigid (6).

To address the issue of core flexibility for a variant tRNA, we have used the method of transient electric birefringence (TEB), in combination with a series of phased tRNA–A_5 bulge constructs (5), to demonstrate that the noncanonical bovine mtRNA^{Ser}(AGY) (Figure 1) possesses substantially more flexibility then its canonical tRNA counterparts. The current work should lead to a better understanding of the interplay between tertiary RNA structure and dynamic flexibility, and suggests that tRNA flexibility, in addition to flexibility within the ribosome, may play a role in the transit of noncanonical tRNAs during the translation cycle. Moreover, the presence of flexibility may broaden the scope of the study of the pathogenic mechanisms of point mutations within these noncanonical tRNAs (7).

MATERIALS AND METHODS

Preparation of extended tRNA–bulge heteroduplex molecules

Plasmid construction is largely as described earlier (1,4), with modifications for measuring flexibility as described in Friederich *et al.* (6). Duplex deoxyoligonucleotides corresponding to the dihydrouridine (dhU or D) arm (5′) and ribothymidine–pseudouridine–cytidine (TψC or T) arm (3′) halves of the tRNA molecule (Table 1) were synthesized and cloned into plasmids pGJ122A and pGJ122B, which code for the 70 bp extensions with a central 'Hind III' insertion site (4). Deoxyoligonucleotides containing the A_5 bulge, and varying numbers of base pairs for the

*To whom correspondence should be addressed. Tel: +1 530 754 7266; Fax: +1 530 754 7269; Email: pjhagerman@ucdavis.edu

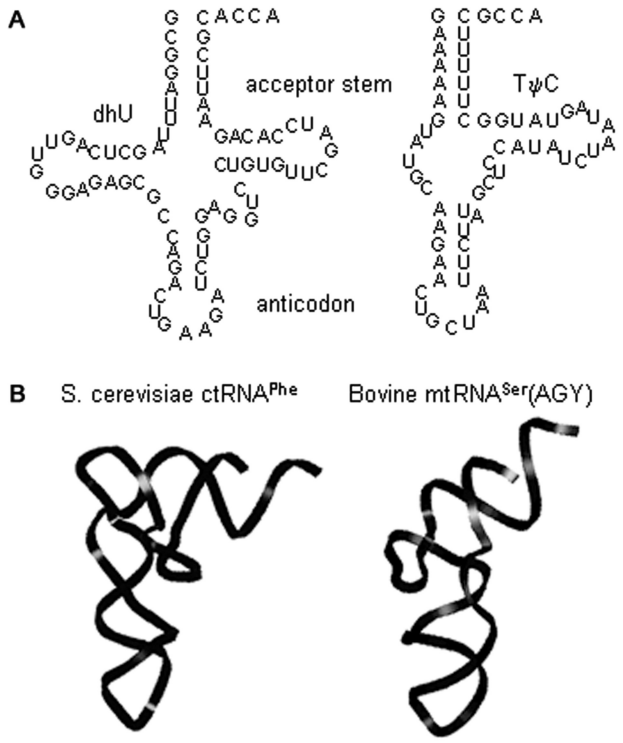

Figure 1. Secondary and tertiary structure of one canonical and one non-canonical tRNA. Ribbons represent phosphate backbone of: yeast cytoplasmic (c) $tRNA^{Phe}$ from Holbrook *et al.* (16), bovine $mtRNA^{Ser}(AGY)$ from Steinberg *et al.* (24), and S. Steinberg (personal communication).

purpose of phasing, (N_n), were cloned into the 5′ side of the D arm and the 3′ side of the T arm using a unique Nhe I site. Linear controls of the designated contour lengths were created by the insertion of specific lengths of deoxyoligonucleotides that did not contain any heteroduplex elements (Table 2). Plasmids were linearized with 'Sma I' prior to transcription with T7 RNA polymerase. Transcription reactions were carried out essentially as described (1). The typical reaction utilized 100 μg of linearized plasmid per 1 ml reaction volume. The reaction buffer also contained 40 mM Tris–HCl (pH 8.1), 4 mM of each rNTP, 1 mM DTT, 0.01% (v/v) Triton X-100 and 20 mM $MgCl_2$ and T7 RNA polymerase (2–6 μg/ml reaction volume). Individual transcripts were annealed and then gel purified (1).

Structure probing by primer extension

As the constructs used were *in vitro* products, structure probing analysis was performed to verify the presence of the expected secondary structure elements (loops and stems). The secondary structure of the *in vitro* transcript representing the single-bend $mtRNA^{Ser}(AGY)$ species, has been verified as demonstrated previously (1). The secondary structure of the extended tRNA–A_5 bulge two-bend constructs was verified in a similar manner using chemical modification probing by the method of Krol and Carbon (8), as described in Frazer-Abel and Hagerman (1), and modified to utilize nonradioactive methods. The presence of single and double stranded regions was verified by probing with dimethylsulphate (DMS), which modifies exposed adenosine residues. Specifically, 4 μg of gel purified tRNA–A_5 bulge construct was incubated in 200 μl of DS buffer (50 mM NaP_i pH 7.2, 1 mM Na_2EDTA, 3 mM $MgCl_2$, 10% glycerol) with 1.2 μl DMS, for 1.5 h at 4°C. After ethanol precipitation, the DMS reaction products were resuspended in DS buffer and further desalted by passage over 1 ml G-25 spin columns equilibrated in the same buffer without glycerol. The reactions were then phenol extracted, reprecipitated and finally resuspended in H_2O. The probing reactions were then annealed to 5′-fluorescein label primers (fluorescein phosphoramidite, Glen Research, Sterling VA), which were designed to anneal to the extensions specifically on the D or T half as described in Frazer-Abel and Hagerman (1). In all other respects, reactions and primer extension analyses are as described previously (1,4,6).

Measurement of relative electrophoretic mobilities

Analytical acrylamide gels (8% acrylamide; 29:1 monomer/bis-acrylamide) were used to examine the relative mobility of the RNA heteroduplex constructs. The gel/running buffer contained 10 mM NaP_i, pH 7.2, with either 1 mM Na_2EDTA or 1 mM Na_2EDTA plus $MgCl_2$ to yield the effective $MgCl_2$ concentration designated in the text (5). The running buffer was recirculated during electrophoresis, and gels were run at room temperature overnight at 30 mA in 17 cm vertical gels.

TEB methodology and measurements

Principle of the TEB method. The method measures the rotational decay times for a linear or heteroduplex DNA or RNA molecule by monitoring the loss of solution birefringence (optical anisotropy) following removal of an orienting electric field pulse. The method exploits the fact that rotational reorientation is extremely sensitive to changes in length of extended molecules in solution (9–11). In a typical experiment, a transient (~1 μs) electric pulse is applied to the sample cell, which aligns the nucleic acid construct. Once the electric pulse is removed, the solution becomes isotropic as the previously oriented molecules randomize through Brownian motion. For heteroduplex species, the sensitivity of the TEB method can be dramatically increased by extending the helices that flank the central nonhelical structure (Figure 2 of ref. 9). The rate of birefringence decay for a given heteroduplex construct is compared to the decay of a fully duplex species of equivalent axial length. The ratio of the decay times is the outcome of the birefringence experiment, and is related to the apparent angle of the central bend. If the bend in the experimental construct possesses additional flexibility (i.e. more flexibility than an equivalent length of pure helix), this will also lead to a reduction in decay time. To remove this ambiguity, a second nonhelical element is added to the construct; in the current instance, A_5 bulge whose angle has been reported elsewhere (12).

The specific methods employed for the measurement and analysis of the birefringence decay curves have been described (4,11,13,14). For the current measurements, the pulse width was 1.0 μs; pulse repetition frequency, 1 Hz;

Table 1. Oligonucleotides used in the production of the single-bend and the tRNA–A_5 bulge constructs

Single-bend oligonucleotides[a]	
dhU half	AGCTGGCGAAAAAGTATGCAAG
pDbmAGY	CCGCTTTTTCATACGTTCTCGA
TψC half	AGCTCTATGCTCCCATATCTAATAGTATGGCTTTTTCGCC
pTbmAGY	GATACGAGGGTATAGATTATCATACCGAAAAAGCGGTCGA

Two-bend parent oligonucleotides[b]	
dhU half	AGCTGGCGAAAAAGTATGCAAGAGCT
pGJ122FD	CCGCTTTTTCATACGTTCTCGATCGA
TψC half	AGCTAGCTCTATGCTCCCATATCTAATAGTATGGCTTTTTCGCC
pGJ122FT	TCGAGATACGAGGGTATAGATTATCATACCGAAAAAGCGGTCGA

n[c]	dhU half[d]	TψC half	Plasmid designation[e]
0	CTAGCAAAAAGCG	CTAGCGCG	pGJ122FB0
	GTTTTTCGCGATC	GCGCGATC	pGJ122FT0
2	CTAGCGCAAAAAGCG	CTAGCGCGCG	pGJ122FB2
	GCGTTTTTCGCGATC	GCGCGCGATC	pGJ122FT2
4	CTAGCGAGCAAAAAGCG	CTAGCGAGCGCG	pGJ122FB4
	GCTCGTTTTTCGCGATC	GCTCGCGCGATC	pGJ122FT4
6	CTAGCCTGAGCAAAAAGCG	CTAGCCTGAGCGCG	pGJ122FB6
	GGACTCGTTTTTCGCGATC	GGACTCGCGCGATC	pGJ122FT6
8	CTAGCAGCTGAGCAAAAAGCG	CTAGCAGCTGAGCGCG	pGJ122FB8
	GTCGACTCGTTTTTCGCGATC	GTCGACTCGCGCGATC	pGJ122FT8
10	CTAGCGCAGCTGAGCAAAAAGCG	CTAGCGCAGCTGAGCGCG	pGJ122FB10
	GCGTCGACTCGTTTTTCGCGATC	GCGTCGACTCGCGCGATC	pGJ122FT10
12	CTAGCTAGCAGCTGAGCAAAAAGCG	CTAGCTAGCAGCTGAGCGCG	pGJ122FB12
	GATCGTCGACTCGTTTTTCGCGATC	GATCGTCGACTCGCGCGATC	pGJ122FT12
14	CTAGCGATAGCAGCTGAGCAAAAAGCG	CTAGCGATAGCAGCTGAGCGCG	pGJ122FB14
	GCTATCGTCGACTCGTTTTTCGCGATC	GCTATCGTCGACTCGCGCGATC	pGJ122FT14
18	CTAGCTAGAGATAGCAGCTGAGCAAAAAGCG	CTAGCTAGAGATAGCAGCTGAGCGCG	pGJ122FB18
	GATCTCTATCGTCGACTCGTTTTTCGCGATC	GATCTCTATCGTCGACTCGCGCGATC	pGJ122FT18

[a]Oligonucleotides used to create the wild-type bovine mtRNA(AGY) used in temperature studies (1).
[b]Parent oligonucleotides used to create the parent species that was annealed and inserted into *Hind III* site of pGJ122A or pGJ122B.
[c]n, the number of additional (phasing) bases. The additional bases are underlined.
[d]Oligonucleotides used to create each species by annealing and insertion into the *NheI* site of corresponding parent plasmids.
[e]pGJ122 corresponds to the original plasmid, B, bulge (dhU) side; T, TψC side, numbers correspond to the number of phasing bases added.

orienting field strength, 10 kV/cm; the instrument response time, $\leqslant$20 ns (buffer birefringence decay). Measurements of the single-bend construct were performed at 3.8 ± 0.1, 20.8 ± 0.1 and 37.4 ± 0.1°C as indicated. For the two-bend constructs, measurements were performed at 3.5 ± 0.1°C, in 5 mM NaP_i pH 7.2 with 1 mM Na_2EDTA or with 1 mM Na_2EDTA and with the necessary $MgCl_2$ to yield the indicated effective free concentrations of $MgCl_2$. Each birefringence decay curve represents the average of 128 transients, which were digitized and averaged on a LeCroy 9310 oscilloscope. Sets of five decay curves were obtained for each construct for each experimental run, and a minimum of two experiments were run for each condition on two independent RNA preparations for a total of $\geqslant$10 decay curves per sample. Decay curves were analyzed as double-exponential

Table 2. Sequences of oligonucleotides used to create linear (duplex) controls[a]

RNA species plasmid designations[a]	Oligomer sequences[b]
158 linear	
pDL158	5′-AGCTGGCGAAAAAGTATGCAAG
pTL158	CCGCTTTTTCATACGTTCTCGA-5′
170 linear	
pDL170	5′-AGCTAGCGCGCTAGCTCTTGCATACTTTTTCGCC
pTL170	TCGCGCGATCGAGAACGTATGAAAAAGCGGTCGA-5′
174 linear[b]	
pGJ122A38+	5′-AGCTGGTGCGGATAGTCTGCAGCATCATGACCAGAGCT
pGJ122B38-	CCACGCCTATCAGACGTCGTAGTACTGGTCTCGATCGA-5′
182 linear	
pDL182	5′-AGCTAGCTAGCAGCTGAGCGCTAGCTCTTGCATACTTTTTCGCC
pTL182	TCGATCGTCGACTCGCGATCGAGAACGTATGAAAAAGCGGTCGA-5′
188 linear	
pDL188	5′-AGCTAGCGCGCTAGCTCTGGAGGTCCTGTGTTCGATCCACAGAATTCGCACC
pTL188	TCGCGCGATCGAGACCTCCAGGACACAAGCTAGGTGTCTTAAGCGTGGTCGA-5′
192 linear	
pDL192	5′-AGCTAGCGAGCGCGCTAGCTCTGGAGGTCCTGTGTTCGATCCACAGAATTCGCACC
pTL192	TCGCTCGCGCGATCGAGACCTCCAGGACACAAGCTAGGTGTCTTAAGCGTGGTCGA-5′
194 linear	
pDL194	5′AGCTAGCCTGAGCGCGCTAGCTCTGGAGGTCCTGTGTTCGATCCACAGAATTCGCACC
pTL194	TCGGACTCGCGCGATCGAGACCTCCAGGACACAAGCTAGGTGTCTTAAGCGTGGTCGA-5′

[a]Pairs of plasmids are created with the same insert, with opposite orientations in the two plasmids.
[b]See Friederich *et al.* (4).

functions using the Levenberg–Marquardt method. For additional analysis of error, refer Hagerman and Hagerman (13).

Interpolation of decay times for linear duplex RNA constructs

For the current studies, five linear constructs (dplx) were utilized to accompany the 10 heteroduplex constructs (htx) containing the tRNA core and the A_5 bulge. To allow the proper determination of the τ ratios (τ_{htx}/τ_{dplx}), it was necessary to determine τ_{dplx} values for linear controls of the same contour length for each construct. The estimation of the effective contour length of the tRNA core for bovine mtRNA^{Ser} (AGY) has been described in detail (1) and determined to be 163 bp. To determine the τ_{dplx} value for linear species of 163 bp, the τ_{dplx} values for the four linear species actually measured were interpolated (Figure 2A and B). Figure 2A demonstrates the fit for each of the conditions presented in Tables 3 and 4. In Figure 2B, the data points for all temperatures were corrected to 20°C and replotted using the following conversion formula:

$$\tau_{20,w} = \tau_{meas}\left(\frac{\eta_{20}}{\eta_T}\right)\left(\frac{T+273}{293}\right)(^{\circ}C)$$

The tight clustering of the data points indicates that the different temperatures were not causing structural alterations in the duplex construct. Decay times for these equivalent duplexes are obtained by interpolation using a set of four duplex species (Tables 3 and 4).

For the two-bend tRNA–A_5 bulge constructs, seven linear species were measured and the τ_{htx} values for intermediate lengths were determined by interpolation (Figure 2C). The results of this interpolation indicate that there were no unexplained or unexpected factors affecting the TEB measurements, and support the use of interpolation to achieve τ-values of intermediate linear length. Additionally, the use of five data points to obtain a single τ-value reduced the influence of sequence variation that might have influenced a single data point.

Hydrodynamic modeling

All hydrodynamic modeling presented is as described (6). The initial hydrodynamic computations utilized the angle measurements shown in Table 5. The first bend, the tRNA core, was modelled as a point bend at base 83 and the second bend at base pair $100 + n$. The other helical parameters used are as follows: twist 12 bp per turn, rise 2.8 Å per bp, hydrodynamic radius 13 Å, helix persistence length (P) 700 Å and helix torsional elastic constant (*C*)

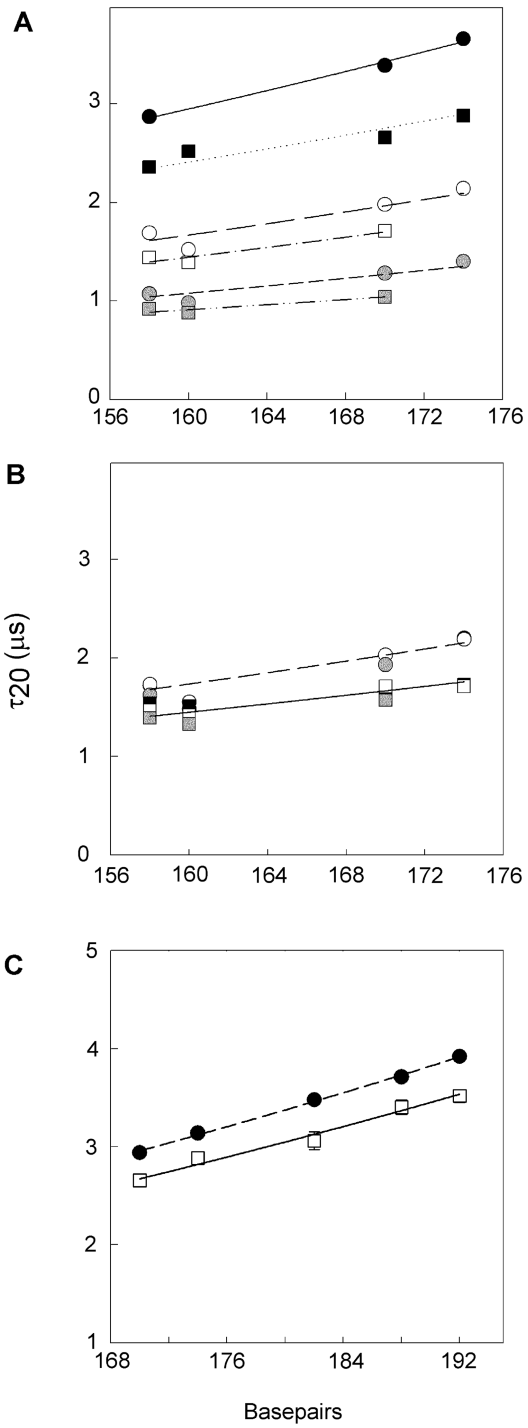

Figure 2. Dependence of the linear length (bp) versus τ-value. Interpolations used for single-bend temperature data presented in panels **A** and **B**: (black circle) 0 mM $MgCl_2$, 3.8°C; (white circle) 0 mM $MgCl_2$, 20.8°C; (grey circle) 0 mM $MgCl_2$, 37.4°C; (black square) 2 mM $MgCl_2$, 3.8°C; (white square) 2 mM $MgCl_2$, 20.8°C; (grey square) 2 mM $MgCl_2$, 37.4°C. All interpolation functions conform to $y = ax^b$, with b held between 2.3 and 2.7 (25). (**A**) Decay times at measured temperature with interpolation plots for each condition. (**B**) All decay times corrected to 20°C and replotted to verify the behaviour of the linear controls under different temperature conditions: dashed line, no magnesium; solid line, 2 mM $MgCl_2$. Interpolation for two-bend flexibility studies. (**C**) Circles represent data obtained in the absence of Mg^{2+}; open squares, data with 2 Mg^{2+}.

3.0×10^{-19} erg cm. To model the data, the last two parameters were altered within the region between base pairs 73 and 93, roughly the expanse of the tRNA core.

RESULTS

Formation and verification of the extended mtRNA^{Ser}(AGY)–A_5 bulge constructs

The construction of the single-bend construct of the bovine mtRNA^{Ser}(AGY) has been described in detail (1). The sequences of the oligonucleotides used to create the single-bend and the two-bend tRNA–A_5 bulge constructs, with the varied spacing (n), are contained in Table 1. The current approach, depicted in Figure 3, is essentially that used in Friederich *et al.* (6), except for the inclusion of three additional phasing sizes: $n = 14$, $n = 16$ and $n = 18$.

The secondary structure of the tRNA core and the presence of the A_5 bulge were verified by chemical modification probing. DMS alkylates the free N1 of adenosine (A) and, to a lesser extent, the N3 of cytosine (C), when those residues are not involved in Watson–Crick base pairing. Figure 4 shows a probing experiment on the phasing construct, $n = 0$, where the mtRNA core and A_5 bulge are in the closest proximity; alkylation of the A and C bases stops reverse transcriptase one base before the modification, as can be seen in the figure. DMS also alkylates N7 of guanosine, but that modification does not stop reverse transcriptase. Similar experiments on the $n = 8$ and $n = 10$ constructs gave similar results, verifying the presence of the A_5 bulge and of the stems and loop expected for the tRNA core.

TEB measurements at increased temperature and in the presence of magnesium reveal increased dispersion in the interstem angle

Measurement of the apparent interstem angle of the single-bend wild-type bovine mtRNA^{Ser}(AGY) were made at both 4°C and 37°C to provide an initial assessment of possible enthalpic contributions to the apparent angle, which would suggest the presence of at least some core and/or interstem stabilizing interactions. Measurements made in the presence of 2 mM magnesium do demonstrate a larger apparent angle and/or greater angle dispersion at the higher temperature (Table 5), suggestive of the loss of some stabilizing interactions that may have been present at the lower temperature in the noncanonical bovine mtRNA^{Ser}(AGY). Measurements made in the absence of magnesium did not vary with temperature, suggesting that such stabilizing interactions are not present in the absence of divalent cations (Table 5).

Absence of a strong phase-dependence of electrophoretic motilities of the tRNA–A_5 bulge constructs is indicative of substantial flexibility in the tRNA core

Heteroduplex RNA constructs containing the bovine mtRNA^{Ser}(AGY) core element and an A_5 bulge, separated by varying numbers of base pairs, were run on polyacrylamide gels (Figure 5, right panels). The weak phase

Table 3. Birefringence decay times and fractional amplitudes[a] for the single-bend tRNA species and linear controls; absence of magnesium

	Fraction fast decay	Fast decay time (μs)	Fraction slow decay	Slow decay time (μs)
4°C[b]				
Bovine mtRNA^{Ser} (AGY)	0.69 (0.01)[c]	0.54 (<0.01)	0.29 (<0.01)	2.30 (0.02)
158 bp linear	0.12 (<0.01)	0.27 (0.01)	0.87 (<0.01)	2.87 (0.02)
170 bp linear	0.16 (<0.01)	0.31 (0.03)	0.82 (0.01)	3.39 (<0.01)
174 bp linear	0.15 (<0.01)	0.34 (0.01)	0.84 (<0.01)	3.66 (0.03)
20°C				
Bovine mtRNA^{Ser} (AGY)	0.72 (0.01)	0.34 (0.01)	0.27 (<0.01)	1.29 (0.12)
158 bp linear	0.08 (<0.01)	0.17 (0.01)	0.91 (<0.01)	1.69 (<0.01)
170 bp linear	0.12 (<0.01)	0.20 (<0.01)	0.87 (<0.01)	1.98 (<0.01)
174 bp linear	0.12 (<0.01)	0.23 (0.01)	0.87 (<0.01)	2.14 (<0.01)
37°C				
Bovine mtRNA^{Ser} (AGY)	0.75 (0.01)	0.23 (<0.01)	0.25 (0.01)	0.83 (0.03)
158 bp linear	0.07 (<0.01)	0.09 (<0.01)	0.92 (<0.01)	1.07 (<0.01)
160 bp linear	0.33 (0.03)	0.17 (<0.01)	0.67 (0.03)	0.98 (0.01)
170 bp linear	0.09 (<0.01)	0.14 (<0.01)	0.90 (<0.01)	1.28 (0.01)
174 bp linear	0.14 (0.01)	0.17 (0.01)	0.85 (0.01)	1.40 (0.01)

[a]TEB measurements were performed as described in Materials and methods section. For each RNA species, the fractional decay amplitudes and times represent at least 10 TEB measurements on two independent RNA preparations.
[b]Precise temperatures are provided in Materials and methods section.
[c]Numbers in parentheses represent standard error.

Table 4. Birefringence decay times and fractional amplitudes[a] for the extended tRNA species and linear controls; presence of 2 mM $MgCl_2$

	Fraction fast decay	Fast decay time (μs)	Fraction slow decay	Slow decay time (μs)
4°C[b]				
Bovine mtRNA^{Ser} (AGY)	0.61 (<0.01)	0.55 (0.01)	0.37 (<0.01)	2.10 (0.10)
158 bp linear	0.19 (<0.01)	0.49 (0.05)	0.80 (<0.01)	2.56 (0.02)
170 bp linear	0.18 (<0.01)	0.34 (0.02)	0.81 (<0.01)	2.66 (0.05)
174 bp linear	0.13 (0.01)	0.20 (0.03)	0.86 (0.01)	2.88 (0.04)
20°C				
Bovine mtRNA^{Ser} (AGY)	0.57 (0.01)	0.29 (<0.01)	0.41 (0.01)	1.29 (0.03)
158 bp linear	0.12 (<0.01)	0.22 (0.02)	0.86 (<0.01)	1.44 (0.01)
160 bp linear	0.22 (<0.01)	0.22 (<0.01)	0.77 (<0.01)	1.39 (<0.0)
170 bp linear	0.17 (<0.01)	0.26 (<0.01)	0.81 (<0.01)	1.71 (<0.01)
37°C				
Bovine mtRNA^{Ser} (AGY)	0.76 (<0.01)	0.24 (<0.01)	0.23 (<0.01)	0.88 (0.04)
158 bp linear	0.09 (<0.01)	0.11 (<0.01)	0.91 (<0.01)	0.92 (<0.0)
160 bp linear	0.18 (<0.01)	0.14 (0.02)	0.81 (0.01)	0.88 (0.02)
170 bp linear	0.11 (<0.01)	0.13 (0.01)	0.90 (<0.01)	1.04 (0.01)

[a]TEB measurements were performed as described in Materials and methods section. For each RNA species, the fractional decay amplitudes and times represent at least 10 TEB measurements on two independent RNA preparations.
[b]Precise temperatures are provided in Materials and methods section.

dependence of the mobilities of the two-bend constructs stands in stark contrast to the large phase dependence observed for the yeast tRNA^{Phe}–A_5 constructs (Figure 5, left panels), for which previous studies demonstrated substantial structural rigidity of the yeast tRNA^{Phe} core (6). The flexibility contributing to the weak phasing must reside in the bovine mtRNA^{Ser}(AGY) core element, since the A_5 bulge is shared for heteroduplex constructs involving both tRNA species. Interestingly, comparison also reveals that while the canonical yeast tRNA^{Phe} constructs exhibit more pronounced phasing in the presence of magnesium than in its absence, the reverse is true for the noncanonical bovine constructs. This latter observation indicates that magnesium is exerting fundamentally different stabilizing effects for the two tRNAs. It should be noted that these effects of magnesium are only revealed with the current two-bend constructs, where phasing is possible. Determination of the exact nature of the magnesium effects is beyond the scope of this work, and additional studies would be necessary to begin to determine whether the structural modulation is specific to magnesium, or is a more general effect of divalent ions.

Table 5. Acceptor-anticodon interstem angles for the extended mtRNA^{Ser}(AGY) constructs

	Interstem angle (degrees)		
Extended tRNA species	4°C[a]	20°C	37°C
No magnesium			
Bovine mtRNA^{Ser} (AGY)	119 (3)[b]	115 (3)	114 (4)
2 mM $MgClB_{2B}$			
Bovine mtRNA^{Ser} (AGY)	134 (4)	131 (2)	145 (8)

[a]Precise temperatures are provided in the Materials and methods section.
[b]Parentheses in table refer to standard error.

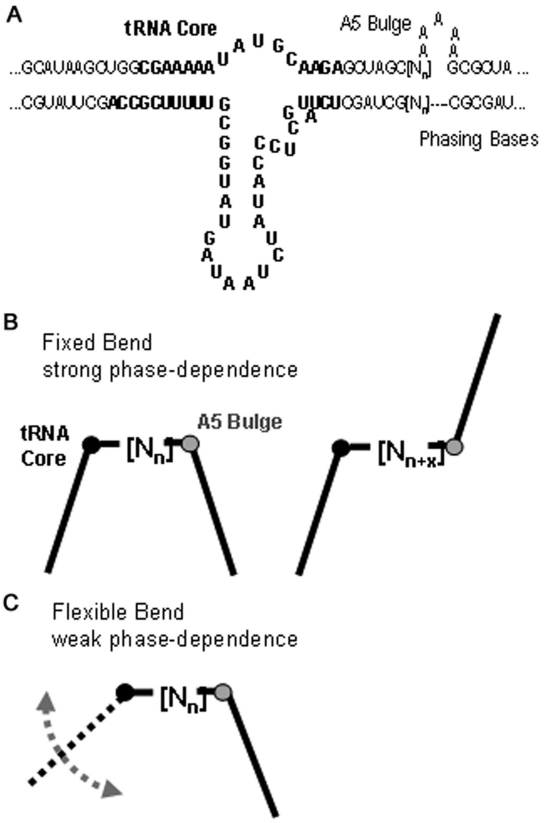

Figure 3. Outline of the construction of double-bend tRNA–A_5 bulge constructs. (**A**) Construction of the tRNA core and A_5 bulge. The phasing bases are indicated as N. The additional extensions are indicated as (dotted line). (**B**) Schematic representation of the phase constructs for a rigid tRNA core, and (**C**) for a flexible tRNA core.

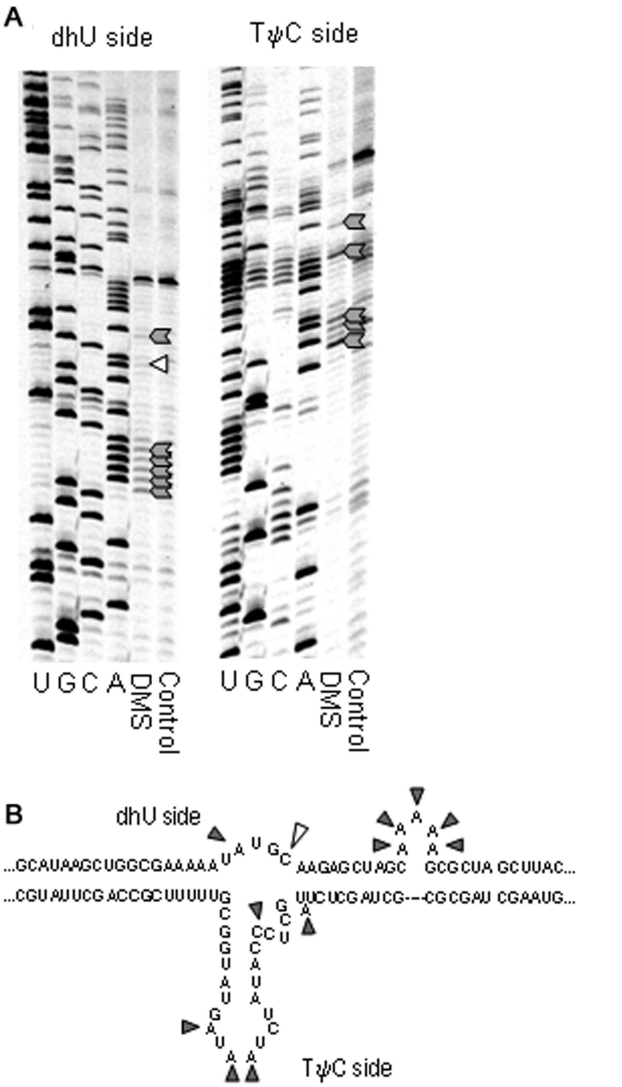

Figure 4. Verification of the expected of secondary structure of the $n = 0$ construct using chemical modification. (**A**) The sites of modification are indicated by closed arrows on the extended secondary structure representation. (**B**) The closed triangles point to sites of modification indicating a single stranded area. The open triangles indicate a site of lesser modification.

TEB decay (τ ratio) measurements for the set of two-bend constructs demonstrate that the bovine mtRNA^{Ser}(AGY) structure possesses substantially greater core flexibility than the canonical yeast tRNA^{Phe}

TEB decay (τ ratio) data for the set of noncanonical bovine mtRNA^{Ser}(AGY) constructs demonstrate only weak phase dependence, indicating that the non-canonical tRNA is flexible (Figure 6). For the canonical yeast tRNA^{Phe}, similar measurements showed a greater than twofold difference between the minimum and maximum τ ratio values in the presence of millimolar quantities of magnesium (6), as predicted for a tRNA core that is as rigid as an equivalent span of duplex RNA helix. For the highly truncated bovine mtRNA^{Ser}(AGY), there was only a 0.6-fold difference, consistent with a substantially flexible mtRNA core.

In Figure 6, curves computed assuming no added core flexibility (6,11) are superimposed on the experimental τ ratio data for the set of two-bend constructs. Although it is difficult to quantify the degree of increased flexibility, since there are likely to be contributions from both reduced torsional and flexural constraints, the dramatic disparity between the theoretical curves and the

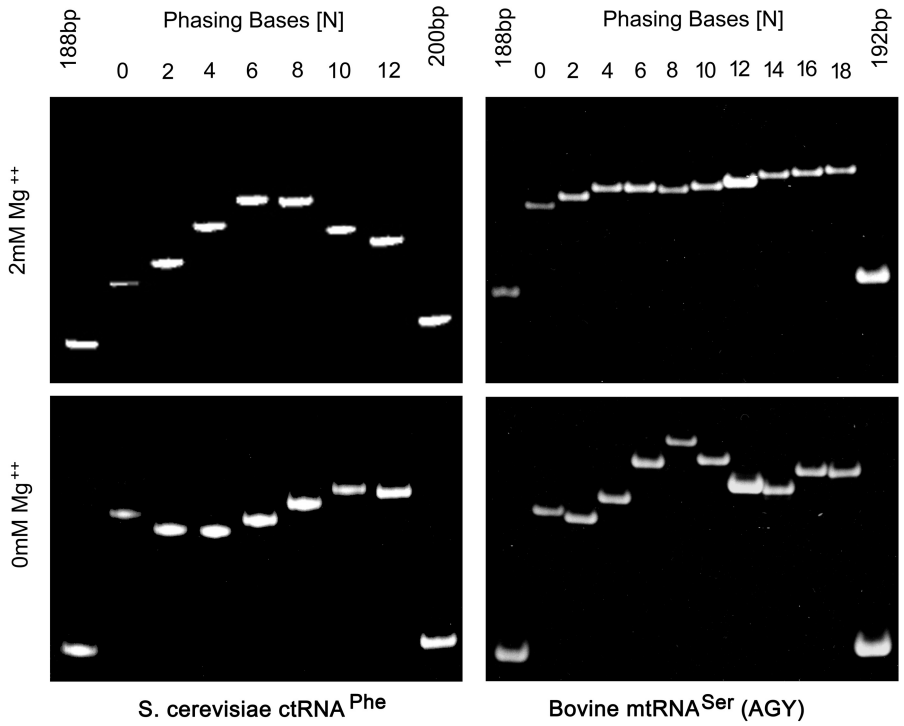

Figure 5. Relative gel electrophoretic mobility. The outside lanes in all gels contain linear duplex controls of the indicated base pairs in length. Numbering of the intervening lanes corresponds to the number of phasing bases added. Gel conditions described in Materials and methods section.

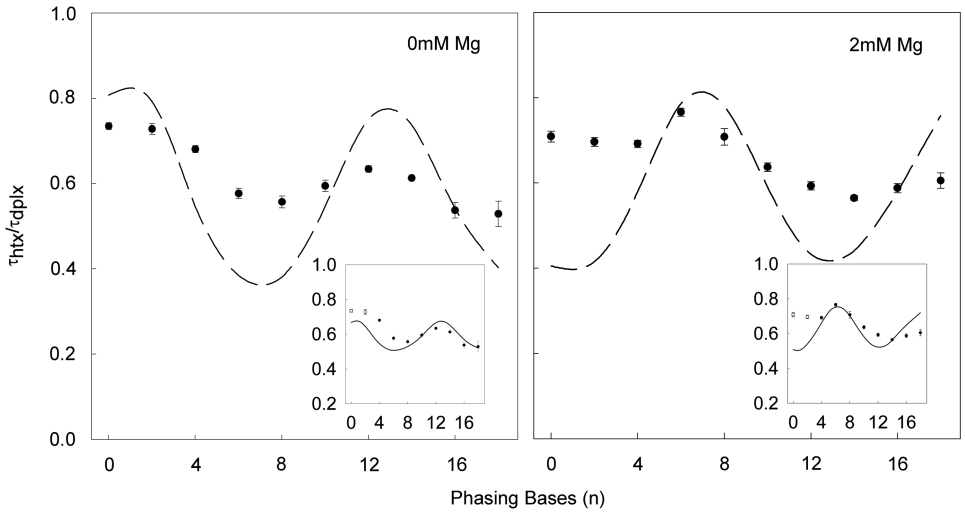

Figure 6. Plots τ ratios as a function of the number of phasing base pairs for the bovine mtRNA^{Ser}(AGY) constructs. Filled circles represent the experimental data. The curve is generated using model values for bend angles (Table 5) with no additional flexibility relative to standard RNA helix ($P = 700$ Å, $C = 3 \times 10^{-19}$ erg cm). (Insets) Computed curves (solid lines) used to model the experimental data for the two-bend tRNA constructs (circles). Parameters used: (no magnesium) true minimum free energy interstem angle 130°, $P = 340$ Å, $C = 0.06 \times 10^{-19}$ erg cm; (2 mM magnesium) minimum free energy interstem angle 150°; $P = 230$ Å, $C = 3 \times 10^{-19}$ erg cm. All theoretical values used were in agreement with the apparent angle measured in the single-bend studies (Table 5).

experimental data clearly indicates that the truncated mtRNA possesses substantially more flexibility than does the canonical tRNA^{Phe} species. Curves computed using the angles reported in Table 5 in effect incorporate an apparent mean angle for the tRNA core that may itself combine both a larger angle of minimum free energy and increased flexibility. Thus, it is difficult to quantify the nature and degree of increased flexibility, since there are likely to be contributions from both reduced torsional and flexural constraints, which render the computational problem underdetermined.

In the insets to Figure 6, the experimental phasing curves are again displayed, along with representative computed curves that approximate the experimental amplitudes.

No attempt has been made to optimize the fit, since the curves are underdetermined with respect to true minimum free energy angles, *P*-values and *C*. However, the total amplitudes of the curves are less than half of the expected values in the absence of added flexibility. For studies in the absence of magnesium, reductions in the torsional elastic constant (*C*) were also incorporated. The improved agreement with the experimental data, while not uniquely defining the nature of the increased flexibility, confirms its presence. The data points represented by open circles ($n = 0$, 2) in the insets to Figure 6 were excluded for reasons that are addressed in the Discussion section.

DISCUSSION

Previous measurements (1,2) of the acceptor-anticodon interstem angles of non-canonical, metazoan mtRNAs, including bovine mtRNA^{Ser}(AGY), revealed two important distinctions between their core angles and the 'L'-shaped form of the archetypal yeast tRNA^{Phe} (5,6,15–17). First, the apparent interstem angles of the truncated mtRNAs are generally greater than that of the nearly right angle of the corresponding angle for yeast tRNA^{Phe}. Second, the core angles for the noncanonical species generally have little if any dependence on the presence of Mg^{2+} ions, in stark contrast to yeast tRNA^{Phe} (5). Despite these differences, it was difficult to draw any definite conclusions regarding the intrinsic rigidity/flexibility of the mtRNA core from the single-bend analyses, since both added flexibility and/or a larger rigid interstem angle would yield similar results for the apparent bend angles (5,6).

In the present work, we have utilized the dual-bend approach used previously by Friederich *et al.* (6), who demonstrated that the yeast tRNA^{Phe} core is intrinsically rigid in the presence of Mg^{2+} ions, but substantially flexible in the absence of divalent cations. For bovine mtRNA^{Ser}(AGY), the more open apparent interstem angle and its relative lack of Mg^{2+} dependence are suggestive of a more flexible core. Indeed, this is born out by the two-bend analysis. What is less clear is the importance and physical properties by which the tRNA bend appears to become more flexible in the presence of Mg^{2+}, than in its absence. Although it would be premature to extend the current conclusions to all truncated tRNAs, the similar patterns of behavior (1,2) for a number of other metazoan mtRNAs suggest a common behavior, perhaps due to a paucity of available interstem interactions.

The current work presents the first evidence of a substantially flexible core for any tRNA species. The presence of additional flexibility is not unexpected, based in part on the lack of available D- to T-loop interactions; however, there has thus far been no direct demonstration of the role of such stabilizing interactions in modulating core rigidity. While a study of tRNA transiting the ribosome has indicated that an abbreviated tRNA would necessarily be flexible in order to accommodate the various stages of transit, measurements have focused on the flexibility of the ribosome (18–22) and not on that of the mtRNA. The markedly reduced phase amplitudes of the experimental curves in Figure 6 relative to expectations for a rigid core, coupled with the minor phase variation of the relative electrophoretic motilities (Figure 5), indicate that the truncated mtRNA is indeed more flexible than the canonical yeast ctRNA^{Phe}. Thus, the process of transit may involve flexibility of both the mitochondrial ribosome and the transiting tRNAs.

The fact that the periodicities of the τ ratio curves (Figure 6) are not uniform may also indicate that the bovine mtRNA is not behaving as a simple hinge, but instead may have a series of discrete conformations. In a mixed pool of conformers, the decay of birefringence due to rotational reorientation would tend to weigh more heavily than the conformations that are more extended in solution because the τ values are derived from the terminal portion of the TEB decay curves. In fact, were the decay curve to reflect a population of slowly interchanging conformers, including *cis*- (fast tumbling, τ ratio minimum) and a *trans*- (slow tumbling, τ ratio maximum) phased species, the resulting apparent τ ratios would be weighted toward larger angles. The possibility of multiple conformers in slow or intermediate exchange (on the time scale of birefringence decay), precludes a quantitative modeling of the nature of the flexibility. Although there is no unique solution for added flexibility, the fundamental conclusion is unambiguous, namely, that the highly truncated mtRNA clearly possesses more flexibility than its canonical counterparts.

Increased flexibility of the bovine mtRNA^{Ser}(AGY) core is consistent with what is known about its secondary structure. This non-canonical tRNA lacks not only many of the conserved residues of the canonical tRNAs, but is also missing one of the arms (DhU arm) of the canonical species. The DhU arm in canonical tRNA is involved in a number of core-stabilizing interactions, including those reinforced by Mg^{2+} ions, that are absent in mtRNA^{Ser}(AGY). Although models for the tertiary structure of bovine mtRNA^{Ser}(AGY) put forth by de Bruijn and Klug (23), as well as models by Steinberg *et al.* (24), do include interactions between the D replacement loop and the T arm, those interactions are not equal in number to those found in canonical tRNA. As suggested by the current work, the proposed interactions in those studies are in any case likely to be insufficient to stabilize the bend to the extent present in canonical tRNA.

Previous work with yeast tRNA^{Phe} has demonstrated the validity of using the two-bend constructs and the τ ratio method to investigate tRNA flexibility (6). In those experiments, where the minimum separation between the two bends was 21 bp, there was a close agreement between the experimental data and the theoretical data derived from independent single-bend measurements. For that study, there was no apparent structural perturbation due to the helical extensions, even when the two arms were nearest to one another, in the *cis*-confirmations (τ ratio minimum). In the current studies, the $n = 0$ and $n = 2$ constructs put the two bends, and consequently two helical extensions, somewhat closer than the 21 bp minimum used for the yeast tRNA^{Phe} measurements; thus, there

may be some as yet unidentified structural interaction for the smallest separations between bend centers. From the structural probing data (Figure 4), the closer proximity of the two bends does not appear to affect the secondary structure within the core region. Because of this remaining question for the most proximal bend centers, the first two data points are depicted as open circles in all the figures.

Bovine mtRNA^{Ser}(AGY) and other metazoan mtRNAs challenge the notion of a universal structure of tRNA. Such differences are clear at the secondary structure level, since the mitochondrial species lacks many of the conserved bases of the canonical tRNA, and lacks one of the arms of the canonical cloverleaf secondary structure. Previous studies demonstrated that the global conformation of the tertiary structure was also quite distinct from that of the canonical tRNA, particularly in the more open interstem angle for the mtRNA. In the current work, we have established for the first time that the core of the non-canonical tRNA possesses substantial flexibility. Thus, at the level of tertiary structure, non-canonical tRNAs are likely to deviate from their canonical counterparts not only in net conformation, but also with respect to the conformational freedom of the core itself.

FUNDING

National Institutes of Health (GM52557 to P.J.H.); Colorado RNA Center Small Grants (A.F.A.). Funding to pay the Open Access publication charges for this article was provided by Departmental funds for P.J.H.

Conflict of interest statement. None declared.

REFERENCES

1. Frazer-Abel,A.A. and Hagerman,P.J. (1999) Determination of the angle between the acceptor and anticodon stems of a truncated mitochondrial tRNA. *J. Mol. Biol.*, **285**, 581–593.
2. Frazer-Abel,A.A. and Hagerman,P.J. (2004) Variation of the acceptor-anticodon interstem angles among mitochondrial and non-mitochondrial tRNAs. *J. Mol. Biol.*, **343**, 313–325.
3. Leehey,M.A., Squassoni,C.A., Friederich,M.W., Mills,J.B. and Hagerman,P.J. (1995) A noncanonical tertiary conformation of a human mitochondrial transfer RNA. *Biochemistry*, **34**, 16235–16239.
4. Friederich,M.W., Gast,F.U., Vacano,E. and Hagerman,P.J. (1995) Determination of the angle between the anticodon and aminoacyl acceptor stems of yeast phenylalanyl tRNA in solution. *Proc. Natl Acad. Sci. USA*, **92**, 4803–4807.
5. Friederich,M.W. and Hagerman,P.J. (1997) The angle between the anticodon and aminoacyl acceptor stems of yeast tRNA(Phe) is strongly modulated by magnesium ions. *Biochemistry*, **36**, 6090–6099.
6. Friederich,M.W., Vacano,E. and Hagerman,P.J. (1998) Global flexibility of tertiary structure in RNA: yeast tRNAPhe as a model system. *Proc. Natl Acad. Sci. USA*, **95**, 3572–3577.
7. Wong,L.J., Yim,D., Bai,R.K., Kwon,H., Vacek,M.M., Zane,J., Hoppel,C.L. and Kerr,D.S. (2006) A novel mutation in the mitochondrial tRNA(Ser(AGY)) gene associated with mitochondrial myopathy, encephalopathy and complex I deficiency. *J. Med. Genet.*, **43**, e46.
8. Krol,A. and Carbon,P. (1989) A guide for probing native small nuclear RNA and ribonucleoprotein structures. *Methods Enzymol.*, **180**, 212–227.
9. Hagerman,P.J. (1996) Sometimes a great motion: the application of transient electric birefringence to the study of macromolecular structure. *Curr. Opin. Struct. Biol.*, **6**, 643–649.
10. Hagerman,P.J. (2000) Transient electric birefringence for determining global conformations of nonhelix elements and protein-induced bends in RNA. *Methods Enzymol.*, **317**, 440–453.
11. Vacano,E. and Hagerman,P.J. (1997) Analysis of birefringence decay profiles for nucleic acid helices possessing bends: the tau-ratio approach. *Biophys. J*, **73**, 306–317.
12. Zacharias,M. and Hagerman,P.J. (1995) Bulge-induced bends in RNA: quantification by transient electric birefringence. *J. Mol. Biol.*, **247**, 486–500.
13. Hagerman,K.R. and Hagerman,P.J. (1996) Helix rigidity of DNA: the meroduplex as an experimental paradigm. *J. Mol. Biol.*, **260**, 207–223.
14. Hagerman,P.J. and Zimm,B.H. (1981) Monte-Carlo approach to the analysis of the rotational diffusion of wormlike chains. *Biopolymers*, **20**, 1481–1502.
15. Hingerty,B., Brown,R.S. and Jack,A. (1978) Further refinement of the structure of yeast tRNAPhe. *J. Mol. Biol.*, **124**, 523–534.
16. Holbrook,S.R., Sussman,J.L., Warrant,R.W. and Kim,S.H. (1978) Crystal structure of yeast phenylalanine transfer RNA. II. Structural features and functional implications. *J. Mol. Biol.*, **123**, 631–660.
17. Sussman,J.L., Holbrook,S.R., Warrant,R.W., Church,G.M. and Kim,S.H. (1978) Crystal structure of yeast phenylalanine transfer RNA. I. Crystallographic refinement. *J. Mol. Biol.*, **123**, 607–630.
18. Guigou,L. and Mirande,M. (2005) Determinants in tRNA for activation of arginyl-tRNA synthetase: evidence that tRNA flexibility is required for the induced-fit mechanism. *Biochemistry*, **44**, 16540–16548.
19. Gutmann,S., Haebel,P.W., Metzinger,L., Sutter,M., Felden,B. and Ban,N. (2003) Crystal structure of the transfer-RNA domain of transfer-messenger RNA in complex with SmpB. *Nature*, **424**, 699–703.
20. Sanbonmatsu,K.Y., Joseph,S. and Tung,C.S. (2005) Simulating movement of tRNA into the ribosome during decoding. *Proc. Natl Acad. Sci. USA*, **102**, 15854–15859.
21. Schuwirth,B.S., Borovinskaya,M.A., Hau,C.W., Zhang,W., Vila-Sanjurjo,A., Holton,J.M. and Cate,J.H. (2005) Structures of the bacterial ribosome at 3.5 Å resolution. *Science*, **310**, 827–834.
22. Yamamoto,T., Izumi,S. and Gekko,K. (2006) Mass spectrometry of hydrogen/deuterium exchange in 70S ribosomal proteins from *E. coli*. *FEBS Lett.*, **580**, 3638–3642.
23. de Bruijn,M.H. and Klug,A. (1983) A model for the tertiary structure of mammalian mitochondrial transfer RNAs lacking the entire 'dihydrouridine' loop and stem. *EMBO J.*, **2**, 1309–1321.
24. Steinberg,S., Gautheret,D. and Cedergren,R. (1994) Fitting the structurally diverse animal mitochondrial tRNAs(Ser) to common three-dimensional constraints. *J. Mol. Biol.*, **236**, 982–989.
25. Hagerman,P.J. (1981) Investigation of the flexibility of DNA using transient electric birefringence. *Biopolymers*, **20**, 1503–1535.